RSC Advances

PAPER

View Article Online
View Journal | View Issue

Cite this: *RSC Adv.*, 2020, **10**, 22570

Development of sulfide, nitrogen co-doping hollow carbon with wideband electromagnetic absorption capability

Wenli Bao, †[ab] Cong Chen†[ac] and Zhenjun Si*[a]

Received 1st May 2020
Accepted 30th May 2020

DOI: 10.1039/d0ra03921g

rsc.li/rsc-advances

Exploration of an economic, easy-producing method to develop high-performance electromagnetic absorber has been a global research interest, owing to the increasingly electromagnetic pollution and interference. In this work, sulfide, nitrogen co-doping carbon (NS–HCS) has been successfully prepared by an *in situ* copolymer and subsequent calcination reaction. The morphologies and phase compositions of these as-prepared samples are analyzed *via* the transmission electron microscopy (TEM), element mappings, X-ray diffraction (XRD) and X-ray photoelectron spectrum (XPS). The result confirms the hollow shaped structure of amorphous carbon is constructed with various types of N, S based covalent bonds. The dotted N and S elements are contribution for the conductive loss and dipole polarization relaxation behavior. The minimum reflection loss value of −34 dB, and effective bandwidth reaches 6.8 GHz with only 1.6 mm. The as-prepared wideband electromagnetic absorber will pave a simple and effective method to obtain lightweight, broadband and thin thickness electromagnetic absorption materials.

1. Introduction

Recently, the extensive application of wireless technology has become a serious social problem, because the yielded electromagnetic radiation is not only possessing a damage to human being's health, but also interfere the operating of neighboring electronics.[1–3] Therefore, there are on-going interests on exploration of electromagnetic absorbing materials, that aims to reduce the electromagnetic pollution by either magnetic or dielectric loss ability.[4] To satisfy the commercial application, an excellent material is requested to be lightweight, high absorption capacity, thin and broad absorption bandwidth and so on.[5,6] Early researches were mainly focused on the magnetic and dielectric hybridized absorbers, such as Fe_3C/Fe_3O_4, $Co_2Fe_2O_4$/graphene, Fe/C *etc.*[7–9] To further strengthen the EM wave absorption ability, continues efforts have been made on the nanostructure, which are also affect the EM absorption performance. However, these reported materials are difficult to satisfy the lightweight feature, which reflected in the big density and higher content of filler.[10] To be specific magnetic/dielectric hybridized absorbers often contains magnetic metal, so that gaining a high density. For certain commercial application, these developed magnetic/dielectric hybridized absorbers should mix with paraffin wax or epoxy resin in a certain weight.[11] Nevertheless, to result in a good EM absorption performance, the weight of magnetic/dielectric hybridized absorber is usually greater than 50 wt%, which will enhance the weight of formed coating layer.[12] In addition, the synthesis of magnetic/dielectric hybridized absorbers involve more than steps.[13] Owing to these drawbacks, it extremely restricts the commercial value of magnetic/dielectric hybridize absorbers.

To get an ideal absorber, more and more interests have been focused on the carbon material. In particularly for the amorphous carbon, it showing moderately permittivity value, controlled dielectric loss ability, easy-production, can be used as a desirable candidate as the electromagnetic absorber.[14–16] Recent progress reveals that producing the hollow nanostructure of carbon not only attributes to the higher EM wave absorption, but also benefits for its low density.[17] Based on the case of Yang group, carbon material designed into hollow one with 230 nm in diameter, the optimized absorption intensity (reflection loss, RL) was nearly −12.5 dB, which was three times stronger than solid one.[18] Qiang *et.al.* reported a yolk–shell shaped C@C microsphere, with an optimized RL value of ∼−39.4 dB.[19] Although showing the improved EM performance, the frequency width with RL < −10 dB is not desirable (<1.0 GHz). It is due to the fact that hollow structure would reduce the dielectric loss value (ε'').[20]

[a]*School of Materials Science and Engineering, Changchun University of Science and Technology, No. 7989, Weixing Road, Changchun, 130022, PR China. E-mail: zdbwl@163.com*

[b]*Criminal Investigation Department, Jilin Police College, Changchun 130117, PR China*

[c]*School of Physics and Electronic Information Engineering, Qinghai Nationalities University, Xining 810007, PR China*

† W.L. Bao and C. Chen contributed equally to this work.

To increase the ε'' value, the method of element doping strategy has been confirmed as the most efficiently and easy way to broaden the absorption. Chen *et.al.* synthesized of sulfide-doped graphene, with an effectively absorption region of 2.0 GHz.[21] Cao *et.al*. explained that the dotted S element graphene has boosted dipole relaxation behavior, thus makes contribution for the EM absorption ability.[22] It is unfortunate that the frequency band for occurring dipole relaxation behavior is always narrow, thus the improvement in ε'' is limited.[23] As for another part of dielectric loss, the conductive loss value still possesses decreases tendency.

To further enlarger the ε'' value, in this article, the S and N dual dotted hollow carbon were successfully made by a facile method, involving the *in situ* polymerization and carbonized method. The role of dotted N and S plays a key role on the conductive loss and dipole relaxation process, which reflected in the increased ε'' value. The optimized sample exhibits a strong EM absorption captivity. We believe that the as-prepared N, S co-dotted hollow carbon sphere can be an ideal candidate as the lightweight, wideband microwave absorber.

2. Experimental

2.1 Synthesis of N, S-co-dotted hollow carbon sphere (SNHC)

The hollow structure with S, N dotted carbon was prepared by a template and solve thermal method, the 200 nm-SiO_2, sulfide and ammonium carbonate ($(NH_4)_2CO_3$) as the templates, sulfide and nitrogen raw. In a typically synthesis of SNHC sample, 2.9 mL of tetraethyl orthosilicate (TEOS) was added into the solution containing 10 mL of H_2O, 30 mL ethanol and 1.5 mL of ammonia aqueous solution ($NH_3 \cdot H_2O$). After stirring 10 min, 0.25 g resorcinol, 0.23 ml of formaldehyde, 0.1 g $(NH_4)_2CO_3$ and 20 mg sulfide were co-added into the above solution and stirring for another 5 min. Afterward, the solution was transferred into a Teflon-lined stainless steel autoclave and heated at 120 °C for 4 h. After naturally cooling to room temperature, the resultant precipitation was washed with ethanol for 3–5 times. The as-prepared precipitation was carbonized at 800 °C, under an N_2 atmosphere or 2 h with a heating rate of 5.0 °C min^{-1}. Lastly, S, N dotted hollow carbon was obtained. For comparison, the S, N dotted solid carbon, N dotted hollow carbon and S dotted hollow carbon have been made, and denoted as SNSC, SHC and NHC, respectively.

2.2 Characterization

The hollow shaped structure and element mappings of these carbon materials are characterized by transmission electron microscopy (TEM; F200F, FEI-Tecnai, USA). The covalent bonds and crystal structures of carbon were recorded *via* an X-ray photoelectron spectroscopy (XPS, PHI 5000 VersaProbe systems), X-ray diffractometer (Bruker D8 ADVANCE X-ray diffractometer) and Raman spectrum (Jobin Yvon HR 800 confocal Rama system). EM characteristics were measured on basis of a coaxial-line theory. In details, the composites used for the EM absorption measurement were prepared by mixing the dotted carbon with paraffin wax in a weight ratio of 10 wt%. Afterwards, a cylindrical shaped sample ($\Phi_{in} = 3.04$ mm, $\Phi_{out} = 7.0$ mm) was produced by hot-pressing the mixture into a specific mold. Subsequent, electromagnetic parameters were tested by the two-port vector network analyzer (VAN, Agilent E5071C). Lastly, the reflection loss value (RL) was calculated, according to following formulas:[24,25]

$$Z_{in} = Z_o(\mu_r/\varepsilon_r)^{1/2}\tan h[j(2\pi fd(\mu_r\varepsilon_r)^{1/2}/c)] \quad (1)$$

$$RL\ (dB) = 20 \log |(Z_{in} - Z_o)/(Z_{in} + Z_o)| \quad (2)$$

where Z_{in} is the input impedance of absorber, f relates to the frequency of electromagnetic wave, d represents the coating thickness of the absorber, while c is the light velocity. ε_r ($\varepsilon_r = \varepsilon' - j\varepsilon''$) and μ_r ($\mu_r = \mu' - j\mu''$) are the complex permittivity and permeability.

3. Results and discussion

Fig. 1a shows the XRD patterns of these carbon materials. Clearly, two characteristic peaks of carbon material at 22.4 and 46° can be observed for N–HCS, S–NCS, NS–SCS and NS–HCS samples. Besides, the diffraction intensity is relatively width, which is attributed to the non-crystalline state. Aiming to gain a deep understanding of the changes of covalent bonds, the FT-IR spectra of pure hollow carbon sphere (denoted as HCS) and NS–HCS are compared in Fig. 1b. As for HCS, typical stretching vibration peaks at 470, 798, 952, 1108, 1405 and 1626 cm^{-1} are corresponded to –C=O, C–C, –C = -C, –COH, –C–H, –COOH bonds,[26] respectively. After dotted by N and S atoms, the C–S, C–SO_4, C–N, C=N and C–N=S are existed at the 864, 1380, 1410, 1572, 1772 cm^{-1}.[27] Due to these S and N-containing covalent bonds, it indicates the N and S have been successfully dotted on the hollow carbon sphere. X-ray photoelectron energy spectra (XPS) was used to detect the NS–HCS sample. In Fig. 2a, evident characteristic signal peaks of N, O, S and C can be obtained from the survey spectra. Meanwhile, the dotted amounts of N and S are 5.6 and 7.9 wt%, respectively. As shown in Fig. 2b, the deconvoluted N1s spectrum have three typical peaks, the first two peaks mainly located at 397.2 and 398 eV, assigning to the pyrrolic and graphitic types of N. Another peak at 398.9 eV is corresponding to pyridine N. The S 2p could be divided into three peaks at 162.2, 163.9, 168.1 eV, which are ascribed to valance bonds of C–S–O, C–SO_x and C–S–C, respectively (Fig. 2c).[28] As plotted in Fig. 2d, the fitted C 1s peaks are corresponding to sp^2 C, C–N, C–O and C–S bonds. Commonly, the exhibited C–S or C–N bonds have a greatly influences on the dielectric behavior, which was due to the existed dipole relaxation behavior.[29]

Apart from the changes of chemical bond, the influence of dotted element on the graphitization level will also plays a key role on in the dielectric behavior, where a higher graphitization can boost the conductivity loss of carbon components and further lead to an enhancement in the total dielectric value. To reveal the varied graphitization degree, Raman spectra of N–HCS, S–HCS, NS–SCS and NS–HCS are provided in Fig. 3. It is clear that all of these samples display two distinguishable

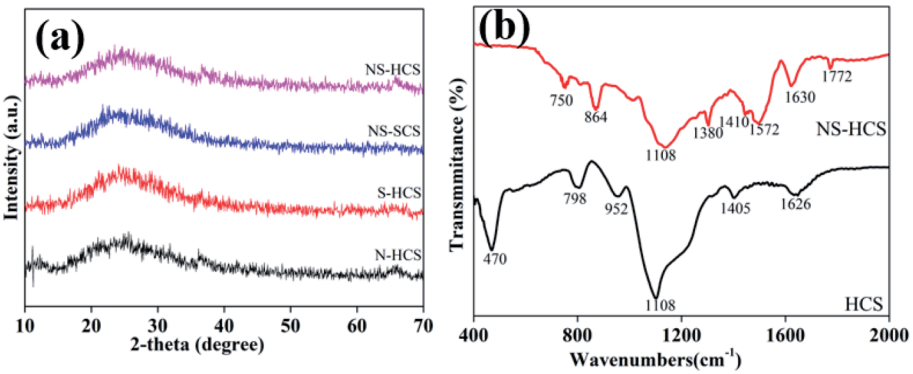

Fig. 1 (a and b) XRD patterns and FT-IR spectra of N, S dotted carbons.

peaks. The two peaks about 1350 and 1590 cm^{-1} can be assigned to the D-band from amorphous carbon and the G-band from graphited carbon.[30–33] Commonly, the ratio of D and G band is stand for the graphitization level. Herein, the D/G ratios of N–HCS, S–HCS, NS–SCS and NS–HCS are estimated to 0.89, 0.9, 0.99 and 0.96, respectively. Hence, it can be deduced that N and S co-dotted carbon have a higher graphitization level. As compared to the solid one, the hollow structure with identical dotted element would lead to the low D/G ratio. According to the dielectric theory, a higher graphitization level can make contribution for the conductive loss. The structural information of the NS–HCS are characterized by TEM image. As seen in Fig. 4a and b, the as-obtained NS–HCS possess a hollow spherical structure with ~210 nm in diameter and 23 nm in shell thickness.

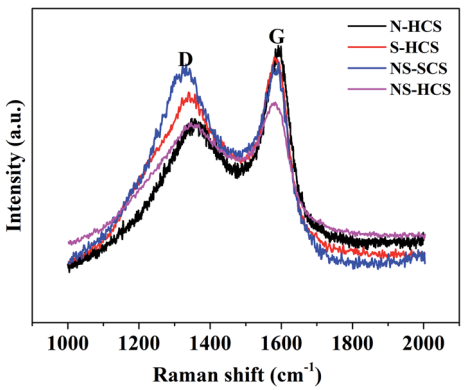

Fig. 3 Raman spectral of N–HCS, S–HCS, NS–SCS and NS–HCS samples.

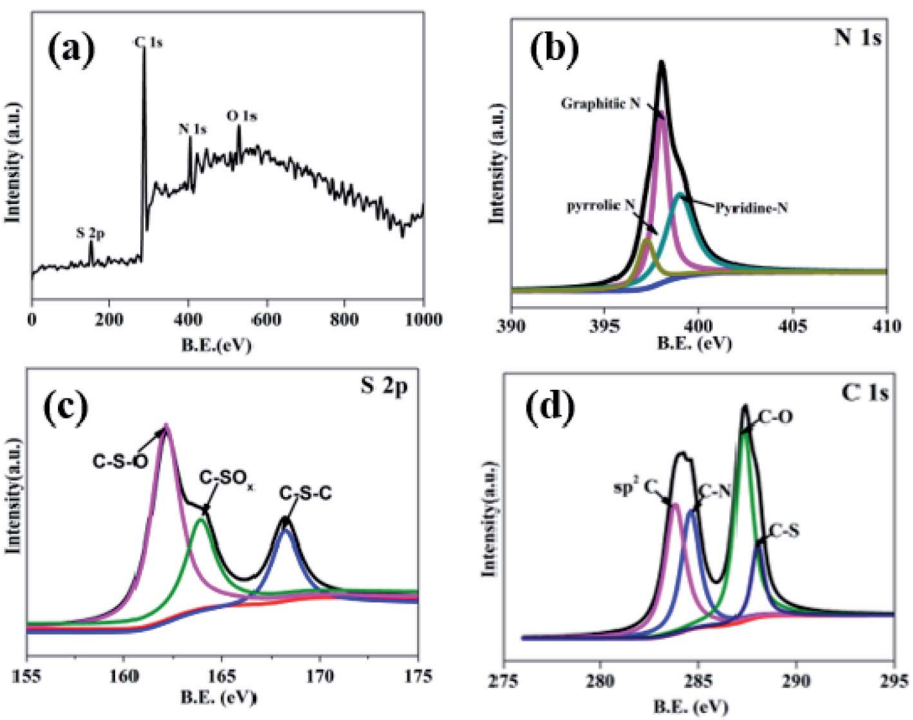

Fig. 2 (a) XPS spectra survey spectrum of the as-prepared NS–HCS sample and high resolution spectra of (b) N 1s, (c) S 2p and (d) C 1s.

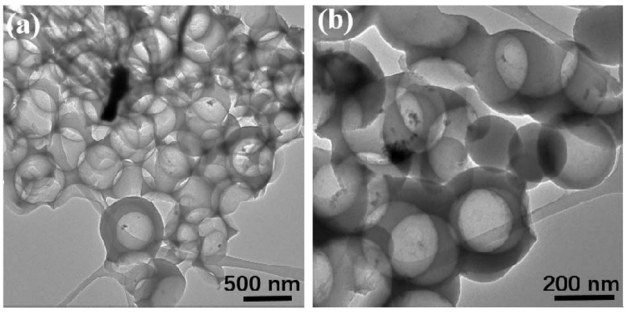

Fig. 4 TEM images and element mappings of NS–HCS sample (a and b).

The permittivity of these dotted carbon composites is measured by the coaxial-line method. The frequency dependent of real part (ε') and imaginary part (ε'') of permittivity are plotted in Fig. 5. Usually, the term ε' is highly associated with the energy storage, and ε'' presents the dielectric dissipation ability, which was attributed to two factors, namely conductivity and polarization relaxation loss.[34–37] As shown in Fig. 5a, ε' value of N–HCS possess a declining tendency from 15.3–12.3 in the whole 2–18.0 GHz region. As compared to N–HCS, ε' of S dotted HCS sample was smaller, but decreasing from 7.8 to 5.3 with increasing frequency, as depicted in Fig. 5b. The ε' of NS–SCS is in the range of 9.3–7.7 over 2–18 GHz with slight fluctuation, which was greater than the S–HCS, as seen in Fig. 5c. As for NS–HCS, it's ε' value slowly decrease from 10.3 to 8.8 (Fig. 5d). It implies that the types of dotted elements greatly affect the ε' value. More importantly, the hollow shaped structure also attributes to a higher ε' value. Concerning ε'' value, N–HCS sample sharply decrease from 7.4 at 2.0 GHz to 6.0 at 8.1 GHz, and then slightly decrease. In whole ε'' curve, it has not any dielectric loss peak, suggesting that conductive loss plays a dominant role on the dielectric loss. When rising the frequency, it is interesting that the ε'' value of S–HCS appears a peak at 8.8 GHz, which would be caused by the dipole relaxation loss behaviors. However, ε'' value of S-dotted HSC is significantly smaller than that of N–HCS. It implies that the HCS dotted by N elements has a larger conductive loss ability, but weaken in the dipole polarization. Similarly, ε'' of NS–HCS and NS–SCS have one dielectric loss peak at 8.7 and 8.9 GHz, respectively. The ε'' value of NS–HCS is 4.0–2.7, which is larger than that of NS–HCS (3.3–2.1). To further confirm the dipole polarization, the Debye relaxation theory has been applied here to discuss polarization mechanism, which can be expressed by the following equation:[38–40]

$$\varepsilon_r = \varepsilon_\infty + \frac{\varepsilon_s - \varepsilon_\infty}{1 + j2\pi f\tau} = \varepsilon' - j\varepsilon'' \quad (3)$$

where ε_s, ε_∞, τ are static permittivity, relative dielectric permittivity at high-frequency limit, and polarization relaxation time, respectively. Whereas, ε' and ε'' can be calculated based on following equations.

$$\varepsilon' = \varepsilon_\infty + \frac{\varepsilon_s - \varepsilon_\infty}{1 + (2\pi f)^2\tau^2} \quad (4)$$

$$\varepsilon'' = \frac{2\pi f\tau(\varepsilon_s - \varepsilon_\infty)}{1 + (2\pi f)^2\tau^2} \quad (5)$$

Based on the eqn (4) and (5), the ε'–ε'' presented as follows:

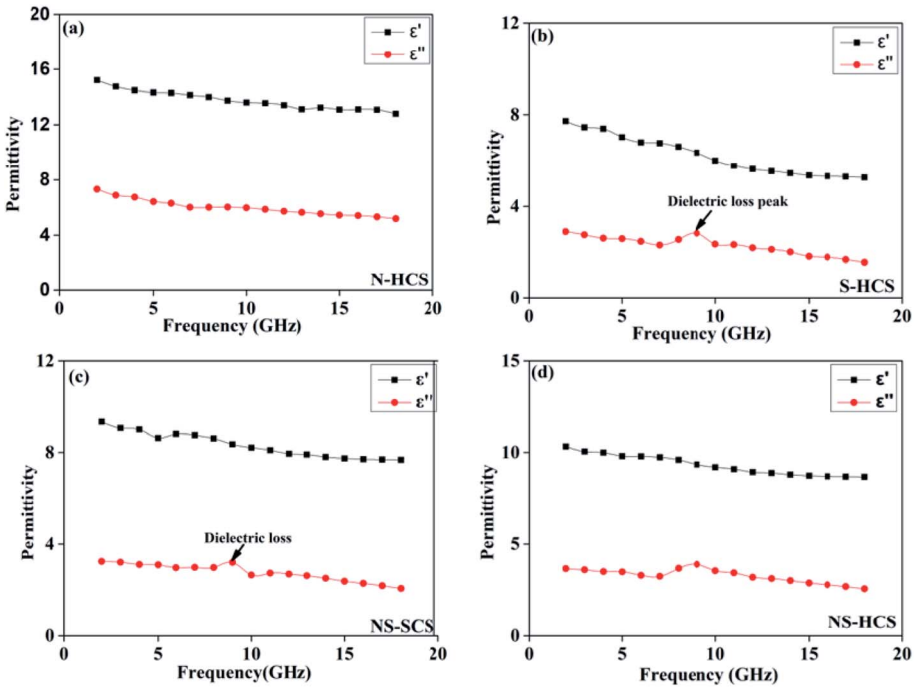

Fig. 5 Frequency dependent of permittivity curves: (a) N–HCS, (b) S–HCS, (c) NS–SCS, (d) NS–HCS.

$$(\varepsilon' - \varepsilon_\infty)^2 + (\varepsilon'')^2 = (\varepsilon_s - \varepsilon_\infty)^2 \quad (6)$$

If the plot of ε'–ε'' exhibits a semicircle, it is related to one Debye polarization relaxation process which make a contribution for ε''. In common, each semicircle corresponds to one Debye relaxation process. Fig. 6 gives the ε'–ε'' curve of these carbon absorber. We can observe that N-dotted HCS has no conspicuous semicircle in the curve, but one for S–HCS, NS–SCS and NS–HCS. Based on the Debye-theory, some conclusions cab be come up as follows:

(1) The dotted S element has a contribution for the dipole polarization relaxation, which would lead to a big ε'' value at high frequency region.

(2) The dotted N element makes a contribution for the conductive loss, and in a result of enhancement of ε'' value.

(3) As compared to solid one, hollow carbon one has a greater ε' and ε'' value.

The enhanced conductively loss would be caused by the enhancing conductivity after adopting N doping strategy. In details, the C replaced by N element possess an improvement of carrier density, it is because that N element has five valence electrons, which is larger than carbon atom (4). Hence, N dotted C actually increase the conductivity, hence reflecting in the higher conductive loss, based on the recent advance. Different from the S element, the radius of N is much closer to C, thus enables to form the graphited N, which inserted into the graphitized area of C and formed three symmetrical C–N covalence bonds. Due to the symmetry, it is not benefits to the dipole polarization. While for S doping, the formed C–S or C–SO_4 dipolar bonds are asymmetric and can act as the dipole center. When giving electromagnetic field, these dipoles are help for the dipole polarization. Considering the structure, the hollow one gaining a higher ε'' value, which may due to the enhanced graphitized degree. It is because that carbon sphere designed into hollow structure, can remarkably increase the specific area. During conducting carbonization reaction, it is easier to gain a high graphitized degree. To evaluate the microwave absorption performance, reflection loss value and response bandwidth are two important points for a desirable absorber, and the effective absorption bandwidth (termed as f_c) will be more important once the RL value lower than −10 dB, because the absorption efficiency is considered to be an acceptable range of 90%.[41–43] In addition, the thickness of absorption thickness is suggested to smaller than 2.0 mm, aiming to satisfy commercial application. On the basis of the tested of permittivity value, the reflection loss (RL) of these carbons can be tested based on the transmission line theory.[44] Fig. 7a shows the calculated reflection curves of N–HCS with a thickness < 2.0 mm in the frequency region of 2–18 GHz. It is noted that the frequency of the RL peak gradually can be driven towards lower frequency region with the increase of thickness. Such a physical mechanism can be fully understood by the quarter-wavelength theory:[45–47]

$$f_R = nc/4d(\varepsilon_r\mu_r)^{1/2} \ (n = 1, 3, 5, 7) \quad (7)$$

where c is the velocity of light, f_R is account for the frequency of absorption peak. It is clearly see that a smaller d would lead to f_R decrease. The minimum reflection loss value of −13.8 dB can be gained at a thickness of 1.9 mm. The effective absorption region equals to 2.4 GHz, at identical 1.9 mm. While for S–HCS, the lowest RL_{min} value of −12. 9 dB appears at 2.0 mm, corresponding f_c is ~1.6 GHz, ranging from 16.4 to 18.0 GHz. When thickness < 2.0 mm, all the RL_{min} values are greater than −10

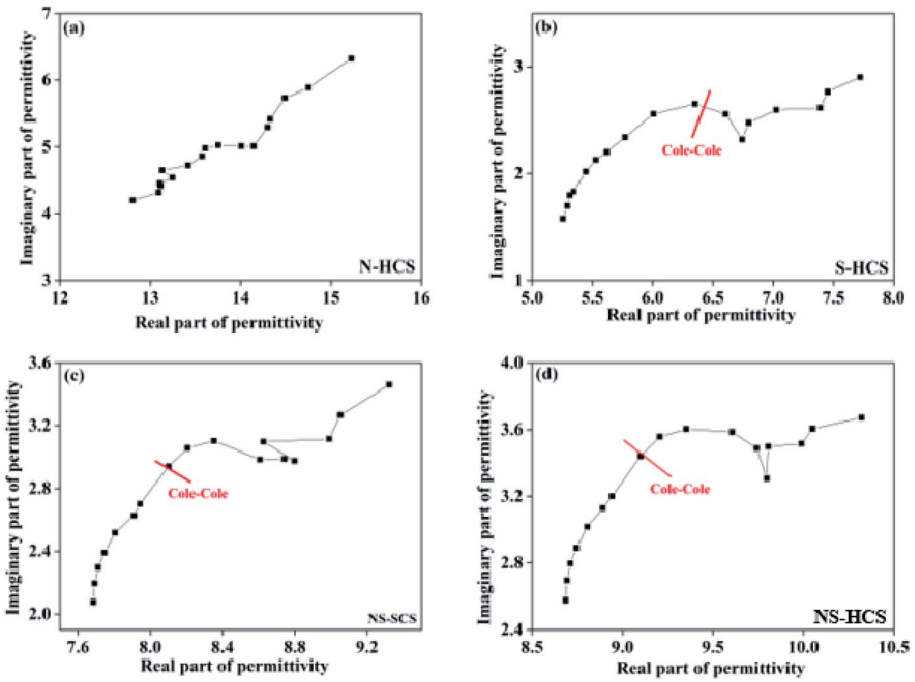

Fig. 6 The corresponding plots of ε'' *versus* ε' for these carbon materials: (a) N–HCS, (b) S–HCS, (c) NS–SCS, (d) NS–HCS.

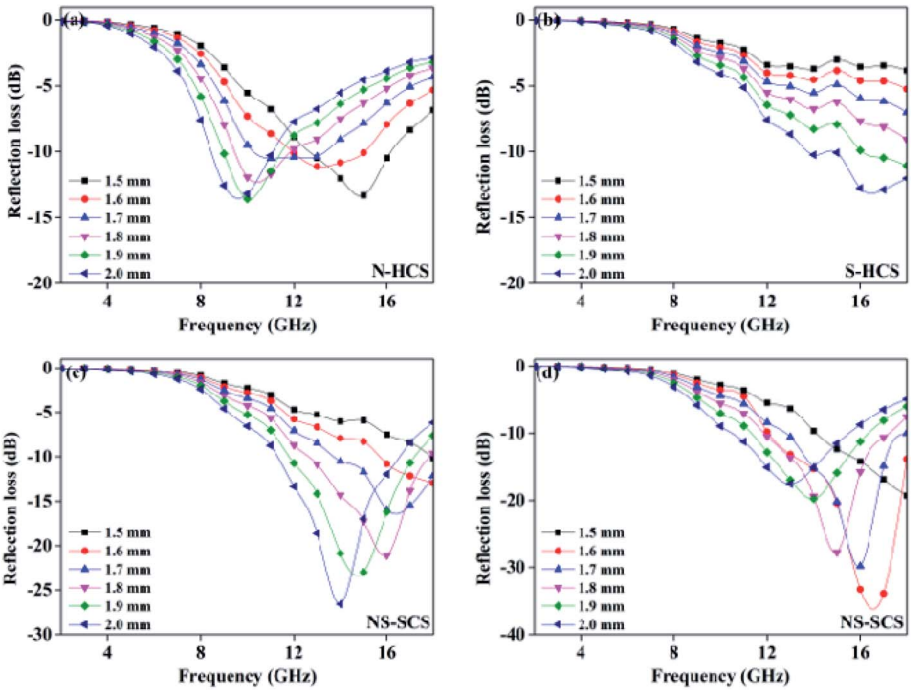

Fig. 7 Frequency dependent of permittivity curves: (a) N–HCS, (b) S–HCS, (c) NS–SCS, (d) NS–HCS.

Table 1 Reflection loss properties of some typical composite of carbon materials

Filler	Matrix	Filler loading ratio (wt%)	RL_{min} (dB)	f_c (GHz)	Range (GHz)	Ref.
3DOC	Wax	5	−45.8 (1.7 mm)	4.8 (1.7 mm)	12.8–17.6	48
MCHS	Wax	20	−50.9 (3.2 mm)	5.4 (3.2 mm)	9.1–14.5	49
C/MQDs	Wax	30	−26.2 (1.5 mm)	5.8 (1.5 mm)	9.0–14.8	50
S Dotted C	Wax	10	−37.3 (2.0 mm)	6.2 (2.5 mm)	11.8–18.0	51
PCHMs	Wax	20	−28.0 (2.6 mm)	3 (2.0 mm)	9–12.0	52
RBC	Wax	10	−59.7 (2.5 mm)	3.4 (2.0 mm)	9.1–12.5	53
PCHMs-10	Wax	10	−51.8 (1.8 mm)	6.0 (1.8 mm)	12.0–18.0	54
NS–HCS	Wax	10	−34 (1.6 mm)	6.8 mm (1.6 mm)	11.2–18.0 GHz	This work

dB, suggesting the performance is unqualified, according to Fig. 7b. In comparison with N–SCS and S–HCS, NS–SCS possesses an improvement RL_{min} value. For example, the smallest RL_{min} value of −26.6 dB under a matched thickness of 2.0 mm. At such thickness, the frequency bandwidth over −10 dB is nearly 6.8 GHz (Fig. 7c). In Fig. 7d, the lowest RL_{min} value of −34 dB can be obtained at a thinner thickness of 1.6 mm only. Meanwhile, this sample exhibits a broad f_c value (covering 11.2–18.0 GHz). Due to the thin thickness, broader f_c and lower RL_{min} value, the NS–HCS can be considered as the optimized sample. We list the reflection loss properties of some typical composite of carbon material (Table 1, ref. 48–54), and it is clear that the excellent performance of NS–HCS sample. With regarding to the RL results, it is easier to find that S and N co-dotted carbon spheres enables an improved EM absorption which were attributed to the synergistic effect of hollow structure and N/S doping.

4. Conclusions

In summary, hollow shaped carbon dotted by N, and S elements have been synthesized by a facile *in situ* polarization method. The results reveal that the carbon sphere designed into hollow shaped structure achieves a higher graphitized level, which was greatly beneficial to the dielectric loss ability. To further stronger the dielectric loss ability, the N, and S element has been adopted on the hollow carbon structure which attributes to the conductive and dipole polarization loss. As a result, the integrated dielectric loss increases significantly, and hence enhancing the electromagnetic absorption performance. Based on the transmission-line measure theory, the optimized RL loss value could up to −34 dB with a f_c of 6.8 GHz under a 1.6 mm. Utilization of element doping on hollow structure has bene confirmed as simple, economic way to development of

lightweight, high performance electromagnetic absorption materials.

Conflicts of interest

There are no conflicts to declare.

Acknowledgements

The authors are grateful for the financial aids from the Science and Technology Foundation of Educational office of Jilin Province (Grant No. JJKHZ-2016-361), Natural Science Foundation of Qinghai Nationalities University (No. 2019XJZ07), and the Natural Science Foundation from Jilin Scientific and Technological Development Program (Grant No. 20170101190JC)

References

1 l. Abdalla, J. Y. Yu, Z. L. Li and B. Ding, *Composites, Part B*, 2018, **155**, 397–404.
2 H. L. Lv, Z. H. Yang, S. J. H. Ong, C. Wei, H. B. Liao, S. B. Xi, Y. H. Du, G. B. Ji and Z. C. J. Xu, *Adv. Funct. Mater.*, 2019, **29**, 1900163.
3 A. L. Feng, T. Q. Hou, Z. R. Jia and G. L. Wu, *RSC Adv.*, 2020, **18**, 10510–10518.
4 A. Elhassan, I. Abdalla, J. Y. Yu, Z. L. Li and B. Ding, *Chem. Eng. J.*, 2020, **392**, 123646.
5 I. Abdalla, A. Salim, M. M. Zhu, J. Y. Yu, Z. L. Li and B. Ding, *ACS Appl. Mater. Interfaces*, 2018, **10**, 44561–44569.
6 H. L. Lv, H. Q. Zhang, J. Zhao, G. B. Ji and Y. W. Du, *Nano Res.*, 2016, **9**, 1813–1822.
7 Z. C. Lou, C. L. Yuan, Y. Zhang, Y. J. Li, J. B. Cai, L. T. Yang, W. K. Wang, H. Han and J. Zou, *J. Alloys Compd.*, 2019, **775**, 800–809.
8 L. Liu, N. He, T. Wu, P. B. Hu and G. X. Tong, *Chem. Eng. J.*, 2019, **355**, 103–108.
9 L. Huang, J. J. Li, Z. J. Wang, Y. B. Li, X. D. He and Y. Yuan, *Carbon*, 2019, **143**, 507–516.
10 X. X. Wang, T. Ma, J. C. Shu and M. S. Cao, *Chem. Eng. J.*, 2018, **332**, 32–330.
11 D. Ding, Y. Wang, X. D. Li, R. Qiang, P. Xu, W. L. Chu, X. J. Han and Y. C. Du, *Carbon*, 2017, **111**, 722–732.
12 Y. Guo, Y. Cheng, L. Y. Wang, B. Zhang, Y. Zhao and Z. Xu, *J. Mater. Chem. C*, 2017, **5**, 491–512.
13 N. Li, G. W. Huang, Y. Q. Li, H. M. Xiao, Q. P. Feng, N. Hu and S. Y. Fu, *ACS Appl. Mater. Interfaces*, 2017, **9**, 2973–2983.
14 C. Q. Song, Y. W. Yin, M. K. Han, X. L. Li, Z. X. Hou, L. T. Zhang and L. F. Cheng, *Carbon*, 2017, **116**, 50–58.
15 Y. Zhang, T. F. Zhang, H. C. Chang, P. S. Xiao, H. H. Chen, Z. Y. Huang and Y. S. Chen, *Adv. Mater.*, 2015, **27**, 2049.
16 X. Bai, Y. H. Zhai and Y. Zhang, *J. Phys. Chem. C*, 2011, **115**, 11673–11677.
17 J. Qiu and T. T. Qiu, *Carbon*, 2015, **81**, 20–28.
18 L. J. Yang, H. L. Lv, M. Li, Y. Zhang, J. C. Liu and Z. H. Yang, *Chem. Eng. J.*, 2020, **392**, 123666.
19 R. Qiang, Y. C. Du, Y. Wang, N. Wang, C. H. Tian, J. Ma, P. Xu and X. J. Han, *Carbon*, 2016, **98**, 599–606.
20 L. L. Yan, M. Zhang, S. C. Zhao, T. J. Sun, B. Zhang, M. S. Cao and Y. Qin, *Chem. Eng. J.*, 2020, **382**, 122860.
21 C. Chen, S. Z. Bao, B. S. Zhang, Y. Y. Zhou and S. M. Li, *J. Alloys Compd.*, 2019, **770**, 90–97.
22 B. Wen, M. S. Cao, M. M. Lu, W. Q. Cao, H. L. Shi, J. Liu, X. X. Wang, H. B. Jin, X. Y. Fang, W. Z. Wang and J. Yuan, *Adv. Mater.*, 2014, **26**, 3484.
23 J. W. Wang, B. B. Wang, A. L. Feng, Z. Jia and G. Wu, *J. Alloys Compd.*, 2020, **83**, 155092.
24 N. Yang, J. Zeng, J. Xue, L. K. Zeng and Y. Zhao, *J. Alloys Compd.*, 2018, **735**, 2212–2218.
25 H. L. Lv, Z. H. Yang, P. L. Y. Wang, G. B. Ji, J. Z. Song, L. R. Zheng, H. B. Zeng and Z. C. J. Xu, *Adv. Mater.*, 2018, **30**, 1706343.
26 L. X. Luo, C. Fu, F. Yang, F. Jiang, Y. Guo, F. Zhu, L. Yang and S. Shen, *ACS Catal.*, 2020, **10**, 1171–1184.
27 J. Zou, H. Shen, Z. Li, S. Zhang, Y. Zhao, X. Bi, Y. Wang, H. Cui and S. Zhuo, *Electrochim. Acta*, 2016, **209**, 557–564.
28 S. F. Huang, Z. P. Li, B. Wang, J. J. Zhang, Z. Q. Peng, R. J. Qi, J. Wang and Y. Zhao, *Adv. Funct. Mater.*, 2018, **28**, 1706294.
29 X. Ma, X. Song, Z. Yu, S. Li and J. S. Gao, *Carbon*, 2019, **149**, 646–654.
30 H. Lv, G. Ji, X. H. Liang, H. Q. Zhang and Y. W. Du, *J. Mater. Chem. C*, 2015, **3**, 5056–5064.
31 G. Wu, Y. H. Cheng, Z. Yang, Z. Jia, H. J. Wu, L. Yang, H. L. Li and P. Z. Guo, *Chem. Eng. J.*, 2018, **333**, 519–528.
32 Y. H. Guo, G. Wu, G. Ji, Y. Zhao and Z. Xu, *ACS Appl. Mater. Interfaces*, 2017, **9**, 5660–5668.
33 X. Zhang, F. Yan, S. Zhang, H. R. Yuan, C. L. Zhu, X. T. Zhang and Y. J. Chen, *ACS Appl. Mater. Interfaces*, 2018, **10**, 24920–24929.
34 H. H. Liu, Y. J. Li, M. W. Yuan, G. B. Sun, H. F. Li, S. M. Ma, Q. L. Liao and Y. Zhang, *ACS Appl. Mater. Interfaces*, 2018, **10**, 22591–22601.
35 H. Lv, X. H. Liang, G. B. Ji, H. Q. Zhang and Y. W. Du, *ACS Appl. Mater. Interfaces*, 2015, **7**, 9776.
36 G. L. Wu, H. X. Zhang, X. X. Luo and L. Yang, *J. Colloid. Inter. Sci.*, 2019, **536**, 548–555.
37 X. Liang, G. Ji, H. Zhang and Y. Du, *ACS Appl. Mater. Interfaces*, 2015, **18**, 9776–9783.
38 Z. C. Lou, R. Li, P. Wang, Y. Zhang, B. Chen, C. X. Huang, C. C. Wang, H. Han and Y. J. Li, *Chem. Eng. J.*, 2020, **391**, 123571.
39 G. Wu, Z. Jia, X. Zhou and G. Z. Nie, *Composites, Part A*, 2020, **128**, 105687.
40 H. L. Lv, Z. H. Yang, H. B. Xu, L. Y. Wang and R. B. Wu, *Adv. Funct. Mater.*, 2020, **30**, 1907251.
41 Y. Li, Z. R. Jia, L. J. Wang, X. Q. Guo, B. Zhao and R. Zhang, *Composites, Part B*, 2020, **196**, 108122.
42 H. X. Zhang, Z. R. Jia, Z. Zhou, C. H. Zhang, K. K. Wang and N. Liu, *Compos. Commun.*, 2020, **19**, 42–45.
43 X. Liang, Y. Cheng, H. Zhang, D. Tang, B. Zhang and Y. Du, *ACS Appl. Mater. Interfaces*, 2015, **7**, 4744–4750.
44 I. Abdalla, J. L. Shen, J. Y. Yu, Z. L. Li and B. Ding, *Sci. Rep.*, 2018, **8**, 12402.

45 X. F. Zhou, Z. R. Jia, A. L. Feng, S. L. Qu, X. Wang, X. H. Liu, B. B. Wang and G. Wu, *J. Colloid Interface Sci.*, 2020, **575**, 130–139.
46 Y. H. Guo, Y. Zhao and Z. Xu, *ACS Appl. Mater. Interfaces*, 2017, **9**, 5660–5668.
47 B. Zhao, J. S. Deng, C. X. Zhao, C. D. Wang, Y. G. Chen and M. Hamidinejad, *J. Mater. Chem. C*, 2020, **8**, 58–70.
48 Y. L. Yu, M. Wang, Y. Q. Bai, B. Zhang, L. L. An, J. Y. Zhang and B. Zhong, *Chem. Eng. J.*, 2019, **375**, 121914.
49 Y. Cheng, Z. Y. Li, Y. Li, S. S. Dai, G. B. Ji, H. Q. Zhao, J. M. Cao and Y. W. Du, *Carbon*, 2018, **127**, 643–652.
50 G. L. Wu, Y. H. Cheng, Z. H. Yang, Z. R. Jia, H. J. Wu, L. J. Yang, H. L. Li and P. Z. Guo, *Chem. Eng. J.*, 2018, **333**, 519–528.
51 Y. Guo, Z. Yang, T. Guo, H. Wu, G. Liu, L. Wang and R. Wu, *ACS Sustainable Chem. Eng.*, 2018, **6**, 1539–1544.
52 H. X. Zhang, B. B. Wang, A. L. Feng, N. Zhang, Z. R. Jia, Z. Y. Huang, X. H. Liu and G. L. Wu, *Composites, Part B*, 2010, **167**, 690–699.
53 H. L. Xu, X. W. Yin, M. H. Li, F. Ye, M. K. Han, Z. X. Hou, X. L. Li, L. T. Zhang and L. F. Cheng, *Carbon*, 2018, **132**, 343–351.
54 H. X. Zhang, Z. R. Jia, A. L. Feng, Z. H. Zhou, C. H. Zhang, K. K. Wang, N. Liu and G. L Wu, *Compos. Commun.*, 2020, **19**, 42–50.